Article

The Alkaline Fusion-Hydrothermal Synthesis of Blast Furnace Slag-Based Zeolite (BFSZ): Effect of Crystallization Time

Changxin Li [1,2,*], Xiang Li [1], Qingwu Zhang [1], Li Li [2] and Shuai Wang [3]

[1] College of Safety Science and Engineering, Nanjing Tech University, Nanjing 211816, China; 1905170120@njtech.edu.cn (X.L.); zqw@njtech.edu.cn (Q.Z.)

[2] College of Chemical Engineering and Pharmacy, Jingchu University of Technology, Jingmen 448000, China; lili@jcut.edu.cn

[3] College of Chemistry and Chemical Engineering, Central South University, Changsha 410083, China; wangshuai@csu.edu.cn

* Correspondence: lichangxin2010@njtech.edu.cn or lichangxin20160706@163.com

Abstract: Blast furnace slag (BFS) is usually regarded as a by-product of the steel industry, which can be utilized as raw material for preparing BFS-based zeolite (BFSZ). In this study, BFSZ was successfully prepared from BFS using alkaline fusion-hydrothermal synthesis. Via the analyses by XRD, SEM, EDX, XRF, FT-IR, elemental mapping and BET/BJH methods, BFSZ crystallization was almost complete at 6 h. With a further increase of crystallization time to 8 h, no significant effect on the formation of crystalline phase was found. Meanwhile, the zeolite content Si/Al (Na/Al) molar ratio was highly affected by crystallization time. The main component of BFSZ prepared at 6 h is cubic crystal with developed surface, with particle size around 2 μm. Moreover, further increasing the crystallization time will not significantly influence the size and morphology of BFSZ product.

Keywords: blast furnace slag; conversion; zeolite; characterization; crystallization time

1. Introduction

According to the data of the National Bureau of Statistics, in 2020, the cumulative output of crude steel in China reached 105.30 million tons, with a cumulative growth of 5.2%. Blast furnace slag (BFS) is usually regarded as a by-product of the steel industry. It is estimated that each ton of iron produced will produce 290 kg BFS [1,2]. There is still a large amount of BFS landfilled in China, because we cannot fully utilize BFS at present [3]. Hence, the landfilled BFS has attracted great attention as regards the pollution of heavy metals and particles in groundwater. Considering this, we urgently need a new way to convert BFS into products of high value-added to meet the requirements of sustainable development in the iron and steel industry.

Recently, the preparation of zeolite from minerals and wastes rich in silicon and aluminum has received great attention, such as ash (fly ash, putty and shell ash) [4–8], clay and slag [9–12] and natural zeolite rock [13,14]. Meanwhile, BFS is rich in silicon and aluminum, which is very suitable for the preparation of zeolite. The zeolite preparation is a heterogeneous reactive crystallization process, and liquid and solid phases generally both exist in the reaction system. The parameters that have the greatest influence on the properties of blast furnace slag-based zeolite (BFSZ) are generally crystallization temperature, crystallization time, initial Si/Al ratio and pressure, etc. In our previous studies, we systematically studied the parameters including crystallization temperature and initial Si/Al ratio in the reaction system on the structure and properties of the BFSZ products. However, further work is needed to clarify all factors controlling the crystal phase and formation of BFSZ. In addition, the crystallization time is known to have a significant effect on the generated crystalline phase and the total crystallinity. Hence, the study of the influence of crystallization time on the synthesis process is very important to clarify and improve the synthesis of BFSZ.

The purpose of this study is to analyze the most effective synthetic route of BFSZ and then to obtain the highest product quality. In order to characterize the synthesized BFSZ, X-ray (powder) diffraction (XRD), scanning electron microscopy (SEM), energy-dispersive X-ray spectroscopy (EDX), X-ray fluorescence (XRF), Fourier transform infrared spectroscopy (FT-IR), elemental mapping and the Brunauer–Emmett–Teller/Barrett–Joyner–Halenda (BET/BJH) methods were utilized to test the BFSZ obtained at different crystallization time.

2. Materials and Methods

2.1. Materials

The BFS samples are collected from multiple positions of a storage yard located in Nanjing, Jiangsu province, China, and then mixed evenly before use. Meanwhile, the same batch of BFS was used to conduct all experiments described in this research. The BFS powder was obtained by passing a 50-mesh sieve after crushing, drying and screening. Table 1 lists XRF analysis results of the BFS used in this study. From Table 1, the main components in the slag were CaO, Al_2O_3, and SiO_2.

Table 1. Determination of chemical composition of blast furnace slag (BFS) and activated BFS (ABFS).

Component	BFS/wt % [a]	ABFS/wt % [a]
CaO	47.08	0.24
SiO_2	29.13	58.59
Al_2O_3	20.59	41.56
MgO	1.11	0.14
Fe_2O_3	1.58	0.58
Na_2O	0.27	0.11
Total	99.76 [b]	99.25 [b]

[a] Measured by X-ray fluorescence (XRF). [b] Sulfur oxides may be present in the remaining components.

2.2. Synthesis of Blast Furnace Slag-Based Zeolite (BFSZ)

Before preparing zeolite, BFS was first activated with nitric acid to obtain activated BFS (ABFS). Namely, 10.0 g of BFS was dissolved in 2.0 mol·L^{-1} HNO_3 solution (100 mL) in a Teflon beaker. After dissolving at 80 °C for 2.0 h, the slurry was filtered to obtain the ABFS (see Table 1 for the chemical components of ABFS). An alkaline fusion-hydrothermal synthesis method was adopted to prepare BFSZ. In a typical program, 1:1.3 (wt %/wt %) ABFS and NaOH was first evenly mixed, after that baked in a muffle furnace at 600 °C for 90 min. Then, 5.0 g of baked products was stirred into 25 mL 1.0 mol/L NaOH (aq) until they were mixed evenly, and 50 mL of aqueous solution containing a certain amount of sodium aluminate or sodium silicate was added to adjust the Si/Al molar ratio to 1:1. The resulting mixture was then transferred to a thermostatic water-bath, stirred at 100 °C for 2 h, and crystallized at the same temperature for a certain crystallization time. Finally, the mixture was filtered, washed with distilled water until neutral and dried for further characterization. To further analyse the impact of crystallization time on the BFSZ synthesis, multiple BFSZ products were produced at different crystallization times.

2.3. Characterization

The XRD pattern of the sample was obtained by D8 discover X-ray diffractometer using Cu Kα radiation in a 5~90° 2θ scan range at 0.02/min scanning rate and operated at 40 mA and 40 kV (D8 discover, Bruker, Berlin, Germany). The samples were chemically analyzed by XRF spectroscopy (Axios, Panalytical, Eindhoven, Holland). The morphological structure of the samples were studied by field-emission scanning electron microscopy (FE-SEM) (SU 8220, Hitachi, Tokyo, Japan) under the following analytical conditions: HV = 20.00 kV, WD = 11.9 mm, HFW = 14.9 μm, mode: SE. ASAP2020 (Micromeritics, Norcross, GA, USA) using N_2 adsorption method was used at 77 K to obtain specific surface area (SSA) through the BET equation. Thermo Scientific Nicolet 6700 FT-IR spec-

trophotometer (Thermo Fisher Scientific, Waltham, MA, USA) was used to perform Fourier transform infrared spectroscopy (using a KBr method) in the 4000–400 cm^{-1} region.

3. Results and Discussion

3.1. Crystalline Characteristics

In this paper, we have systematically investigated the effect of crystallization time on the crystalline characteristics of obtained samples. The XRD patterns of BFSZ samples obtained at various crystallization time are listed in Figure 1. From Figure 1, after 4 h crystallization, NaA zeolite (JCPDS cards number: 71-0784) and ZK-14 zeolite (JCPDS cards number: 84-0698) is present in the products (see Figure 1a), although the diffraction peak intensity is a little weak, indicating incomplete crystallization. As the crystallization time increased to 6 h, the diffraction intensity and crystallinity increased gradually (see Figure 1b). However, as the crystallization time was further increased to 8 h, the diffraction peak was not further strengthened, indicating that the zeolite crystallization was almost completed within 6 h (see Figure 1c). Moreover, the crystallization products obtained at 6 h of crystallization clearly showed some diffraction peaks at 7.19°, 10.18°, 12.47°, 14.41°, 16.13°, 20.43°, 21.69°, 24.01°, 27.14°, 29.97°, 30.86°, 32.58°, 34.22°, 52.66°, 57.60° and 69.22°, which matched well with the characteristic peaks of NaA zeolite (JCPDS cards number: 71-0784) [15–17]. That is to say, the BFSZ obtained at 6 h is mainly composed of NaA zeolite (see Figure 1b). The results showed that NaA zeolite with good crystallinity was successfully formed.
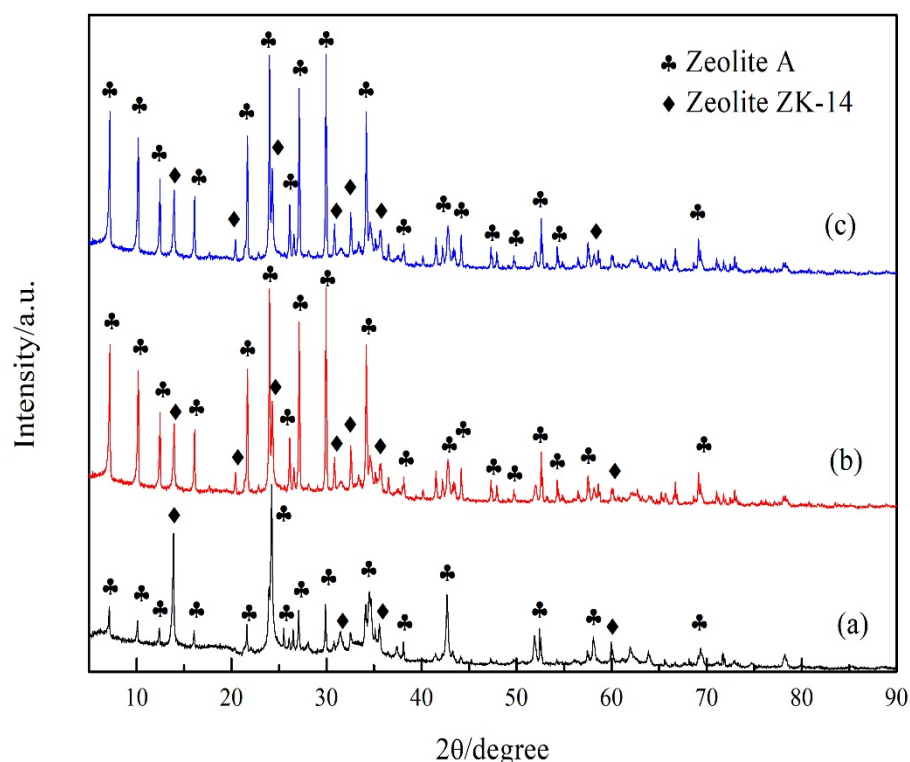

Figure 1. X-ray diffraction (XRD) patterns of the product samples obtained at crystallization time of (**a**) 4 h (**b**) 6 h and (**c**) 8 h.

3.2. Chemical Analysis

The changes of chemical composition and Si/Al (Na/Al) molar ratio are shown in Table 2. Comparing the 0.11% of Na$_2$O content in ABFS, the Na$_2$O content in the BFSZ obtained at various crystallization times were significantly increased. Due to the mechanisms of zeolite growth, the SiO$_4$ tetrahedron can be replaced by Al atoms to form AlO$_4$ tetrahedron. However, the Al atom is trivalent, and the electricity price of one oxygen

atom is not neutralized in the AlO_4 tetrahedron, resulting in charge imbalance, which makes the whole AlO_4 tetrahedron negatively charged. In order to remain neutral, there must be positively charged ions to offset, which are generally compensated for by alkali metal and alkaline earth metal ions, such as Na. Hence, the Na_2O content in BFSZ is changed dramatically. In addition, the great change of Na_2O content is also regarded as other evidence of the successful transformation of BFSZ material [18,19]. The zeolite contents in BFSZ were determined to be 90.90%, 95.53% and 97.41% at crystallization time of 4 h, 6 h and 8 h, respectively. The significant increase on zeolite content of BFSZ samples generally clarify that longer crystallization time is favorable for zeolite formation in the reaction system. On the other hand, Si/Al and Na/Al molar ratio both increases with the increase of crystallization time. Namely, under longer crystallization time, more Si and Na ions are involved in the synthesis of BFSZ. Meanwhile, according to the BFSZ preparation process, Si and Al ions content in the filter liquor recovered after BFSZ preparation at 6 h was determined by ICP (Optima 5300DV, Perkin-Elmer, Waltham, MA, USA). The results show that Al ions concentration in the filter liquor was negligible and Si ions concentration in the filter liquor was 248.68 mg/L. Namely, abundant water-soluble silicates ions are not involved in BFSZ synthesis, while almost all Al ions are involved and consumed in BFSZ synthesis. This phenomenon can be attributed to the fact that during the process of zeolite synthesis, Al acts as the controlling substance and the consumption rate of Al is much higher than that of Si in the reaction. Moreover, there was little change in the relevant data such as chemical component, zeolite content and Si/Al (Na/Al) molar ratio of the BFSZ products prepared at 6 or 8 h. Taking the above results into account, an appropriate crystallization time should be controlled at about 6 h.

Table 2. Chemical components and Si/Al (Na/Al) molar ratio of the obtained BFSZ.

Crystallization Time (h)	Chemical Component [a]/wt %						Molar Ratio		Zeolite Content [b] /wt %
	CaO	SiO_2	Al_2O_3	Na_2O	Fe_2O_3	MgO	Si/Al	Na/Al	
4	0.34	35.42	35.66	19.82	0.65	0.17	0.84	0.90	90.90
6	0.43	38.16	36.76	20.61	0.32	0.09	0.88	0.92	95.53
8	0.36	38.72	36.42	22.27	0.38	0.13	0.90	1.01	97.41

[a] Measured by XRF. [b] Defined by $(SiO_2 + Al_2O_3 + Na_2O)/$ (total weight).

3.3. Fourier Transform Infrared (FT-IR) Analysis

The FT-IR spectroscopy of the BFSZ products obtained are displayed in Figure 2. The band at approximately 544 cm^{-1} was attributed to the external vibration of double four-rings (D4R), which is a feature of NaA zeolite [20–22]. The bands at 440 cm^{-1} and 1030 cm^{-1} are attributed to the vibrations of T–O bending and the TO4 asymmetric stretch (T = Si or Al), respectively. The bands at 3336 cm^{-1} and 1646 cm^{-1} were respectively due to intermolecular hydrogen bond and bonding water [23]. The bands at 711 and 764 cm^{-1} were due to the symmetrical stretching of T–O–T, and a band at 958 cm^{-1} was attributed to the asymmetrical stretching of T–O–T. The results of FT-IR for the BFSZ products obtained were consistent with the interpretation of XRD results.
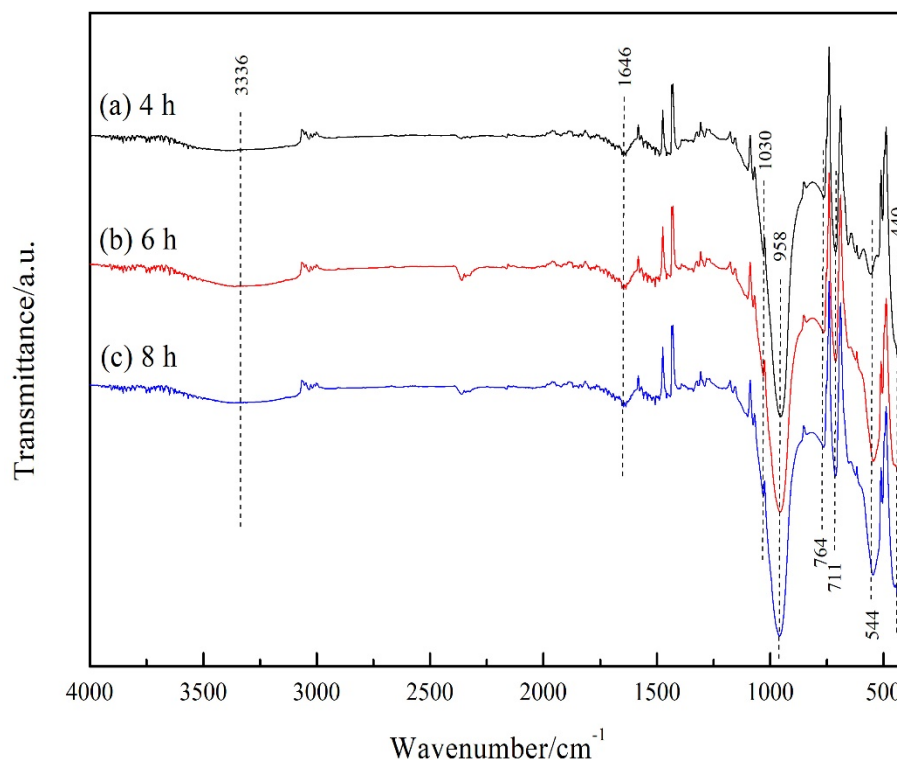
Figure 2. Fourier transform infrared (FT-IR) spectroscopy of the BFSZ prepared at various crystallization time.

3.4. Microstructural Characteristics

The BET/BJH test was carried out to analyze specific surface area (SSA), pore volume and average pore diameter of the BFSZ obtained under various crystallization times. BET/BJH measurements of nitrogen adsorption isotherm and pore size distribution are, respectively, displayed in Figures 3 and 4. Seen from Figure 3, the broad hysteresis loop ranging in $0.2 < P/P0 < 0.8$ and steep elevation in the range of $P/P_0 > 0.8$ indicate the existence of mesoporous and microporous structure [24,25]. Moreover, the pore size distribution in Figure 4 again proves that BFSZ has mesoporous and macropore size pores. Meanwhile, the SSA, pore volume and average pore diameter of the BFSZ are demonstrated in Table 3. Results show that the SSA of the BFSZ became greater with the increase of reaction time. The SSA value for the BFSZ obtained at 6 h or 8 h remain largely unchanged. This again shows that the crystallization time of 6 h is sufficient to prepare BFSZ using the alkaline fusion-hydrothermal method. In addition, the average pore size is usually inversely proportional to the SSA value of BFSZ. This may be because relatively small pores can establish a hierarchical connection system of pores in BFSZ, which may lead to the obtained BFSZ samples having high SSA values.
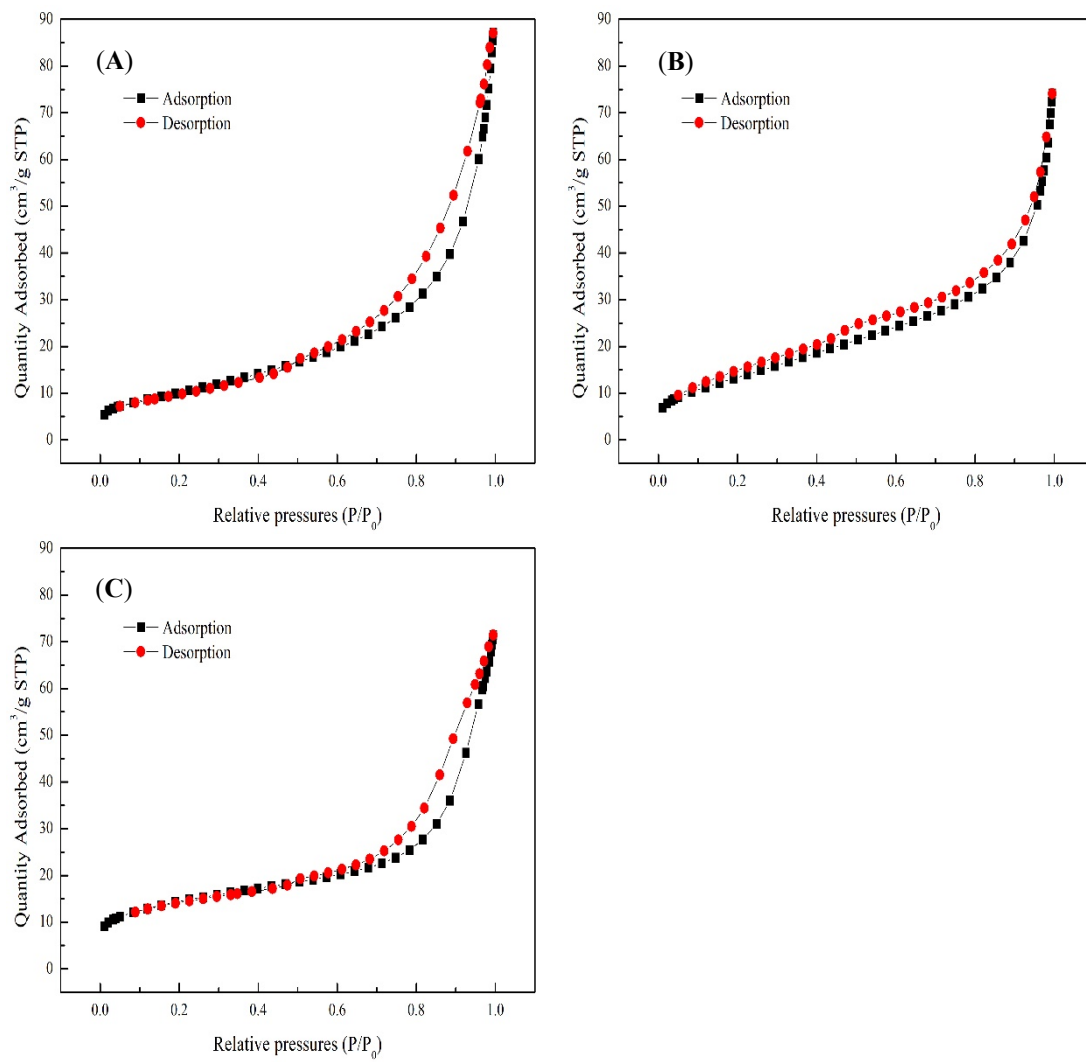
Figure 3. N$_2$ adsorption-desorption isotherms of BFSZ synthesized at crystallization times of (**A**) 4 h (**B**) 6 h and (**C**) 8 h.

Table 3. Microstructural characteristics results of the BFSZ prepared at various crystallization times.

Crystallization Time (h)	SSA (m^2/g) [a]	Pore Volume (cm^3/g) [b]	Average Pore Diameter (nm) [b]
4	37.16	0.14	10.95
6	49.64	0.11	7.62
8	49.96	0.11	7.78

[a] Brunauer-Emmett-Teller (BET) surface area. [b] Determined by Barrett-Joyner-Halenda (BJH) desorption data.
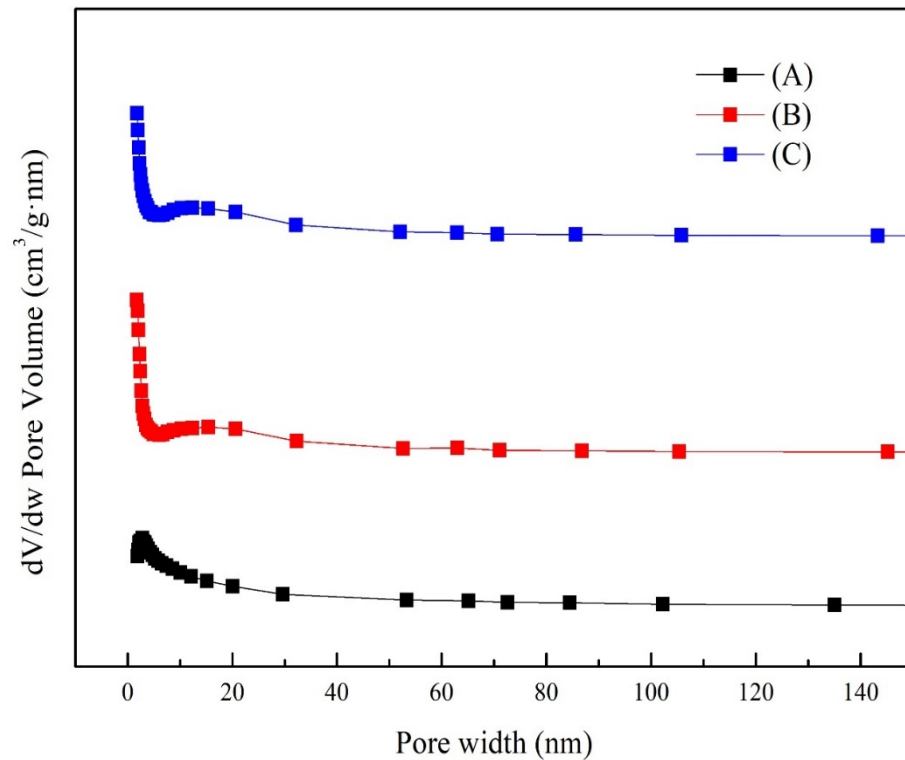
Figure 4. Pore distribution of BFSZ synthesized at crystallization times of (**A**) 4 h (**B**) 6 h and (**C**) 8 h.

3.5. Morphology Analysis

SEM images show that crystallization time has a significant effect on the size and morphology of BFSZ. After 4 h of crystallization, a large number of loosely packed crystals with irregular shapes were discovered, indicating incomplete crystallization. In addition, the morphology listed in Figure 5A again reflected weak peaks displayed in the XRD patterns. As the crystallization time reached up to 6 h, the main component of the product was a much larger cubic crystal with developed surface, and its particle size was about 2 μm (Figure 5B). Moreover, when the crystallization time was further increased to 8 h, all the obtained BFSZ samples were well shaped. In addition, the crystallization time will not significantly affect the crystal size and morphology of the BFSZ (Figure 5C). Moreover, as seen from morphological analyses of BFSZ in Figure 5, the cubic particles with a chamfered shape, along with a small fraction of round crystals can be observed. The cubic and round crystals corresponded to zeolite A and zeolite ZK-14, respectively based on morphology. Moreover, it is worth noting that no aggregates were observed in the SEM pictures which indicate that this shape transformation can provide large surface area with tiny pores. That is to say, 6 h is enough to complete the crystallization process. In addition, with the increase of crystallization time, the surface of BFSZ particles obtained changes from crude to smooth.
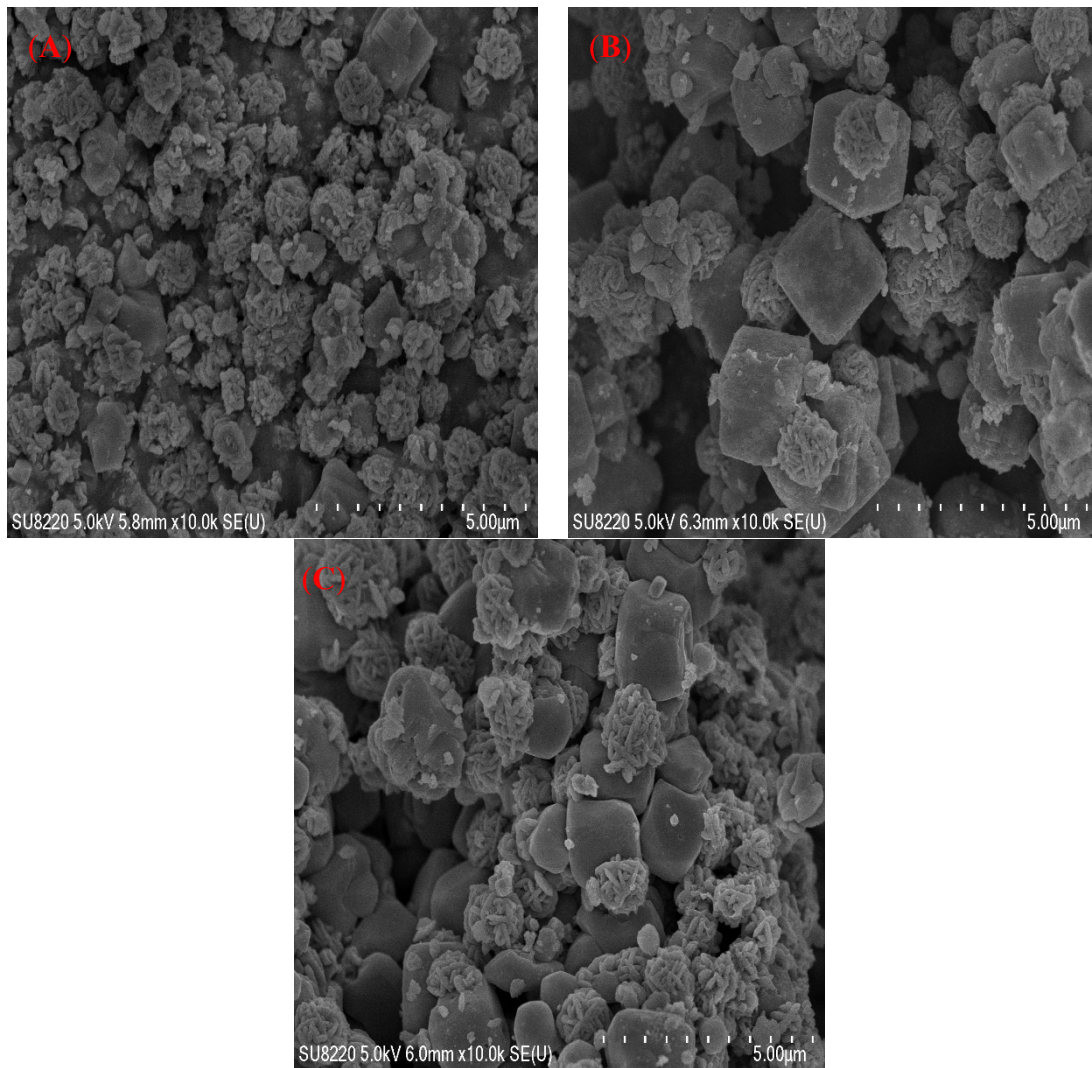
Figure 5. Scanning electron microscope (SEM) images of BFSZ synthesized at crystallization times of (**A**) 4 h (**B**) 6 h and (**C**) 8 h.

3.6. Elemental Mapping Analysis

Elemental mapping analysis was conducted to compare and study the regional (or phase) distribution characteristics of elements in the BFSZ sample obtained under various crystallization times. As seen in Figure 6, the BFSZ sample obtained under various crystallization time contains all BFS-derived metals. As shown in Figure 6A, Si, Al, O and Na-rich phase was formed and the Si, Al and Na were distributed in the same distribution area. From the morphological point of view, this is considered to be zeolite, which once again proves the successful preparation of BFSZ. At the same time, some components such as iron, calcium and magnesium also appear in the mapping image. However, no related crystal structure on iron, calcium and magnesium was discovered in the XRD pattern (see Figure 1). It is likely that those secondary metal ions either cannot form a crystalline phase or may be incorporated into the BFSZ.
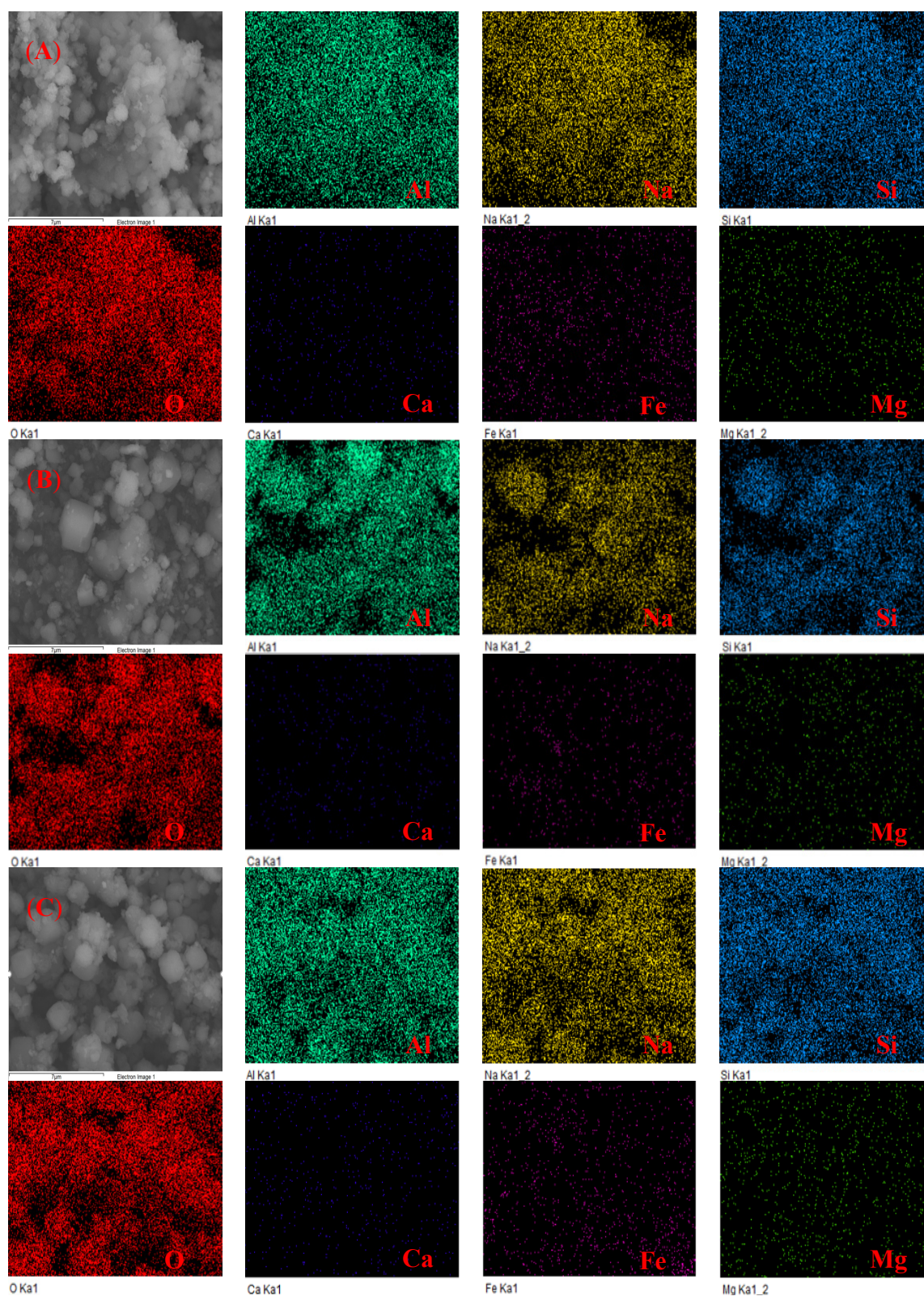
Figure 6. Elemental mapping of BFSZ synthesized at crystallization times of (**A**) 4 h (**B**) 6 h and (**C**) 8 h.

4. Conclusions

The effects of crystallization time on the alkaline fusion-hydrothermal synthesis of BFSZ were investigated. The BFSZ obtained under different crystallization times was measured by XRD, FT-IR, BET/BJH, XRF, FE-SEM and elemental mapping analysis. It

was found that BFSZ crystallization was almost complete for 6 h. A further increase of crystallization time did not have a significant effect on the phase formation. Under 6 h aging, the main phases in BFSZ were NaA zeolite with the average SSA of 49.64 m^2 g^{-1}. Additionally, the cubic crystal with a developed surface in BFSZ crystals with particle size of about 2 μm could be clearly observed. Elemental mapping analysis showed that a Si, Al, O and Na-rich phase was formed and the Si, Al and Na were distributed in the same distribution area. Hence, it can be concluded that the optimal crystallization time for the synthesis of BFSZ using alkaline fusion-hydrothermal treatment is around 6 h. Research on the properties of the obtained BFSZ needs to be conducted through further studies.

References

1. Kuwahara, Y.; Ohmichi, T.; Kamegawa, T.; Mori, K.; Yamashita, H. A novel conversion process for waste slag: Synthesis of a hydrotalcite-like compound and zeolite from blast furnace slag and evaluation of adsorption capacities. *J. Mater. Chem.* **2010**, *20*, 5052–5062. [CrossRef]

2. Ismail, I.; Bernal, S.A.; Provis, J.L.; San Nicolas, R.; Hamdan, S.; Van Deventer, J.S.J. Modification of phase evolution in alkali-activated blast furnace slag by the incorporation of fly ash. *Cem. Concr. Comp.* **2014**, *45*, 125–135. [CrossRef]

3. Tian, P.; Dong, H.W.; Wu, X.M.; Huo, L.Q.; Xue, Y.K. Comprehensive utilization and control measures of iron and steel slag. *Energ. Metall. Ind.* **2020**, *39*, 9–13. (In Chinese)

4. Czuma, N.; Katarzyna, Z.; Motak, M.; Gálvez, M.E.; Costa, P.D. Ni/zeolite X derived from fly ash as catalysts for CO$_2$ methanation. *Fuel* **2020**, *267*, 117139. [CrossRef]

5. Shawabkeh, R.; Al-Harahsheh, A.; Hami, M. Conversion of oil shale ash into zeolite for cadmium and lead removal from wastewater. *Fuel* **2004**, *83*, 981–985. [CrossRef]

6. Kordatos, K.; Gavela, S.; Ntziouni, A.; Pistiolas, K.N. Synthesis of highly siliceous ZSM-5 zeolite using silica from rice husk ash. *Micropor. Mesopor. Mat.* **2008**, *115*, 189–196. [CrossRef]

7. Belviso, C.; Perchiazzi, N.; Cavalcante, F. Zeolite from fly ash: An investigation on metastable behavior of the newly formed minerals in a medium-high-temperature range. *Ind. Eng. Chem. Res.* **2019**, *58*, 20472. [CrossRef]

8. Belviso, C.; Abdolrahimi, M.; Peddis, D.; Gagliano, E.; Sgroi, M.; Lettino, A.; Roccaro, P.; Vagliasindi, F.G.A.; Falciglia, P.P.; Bella, G.D.; et al. Synthesis of zeolite from volcanic ash: Characterization and application for cesium removal. *Micropor. Mesopor. Mat.* **2021**, *319*, 111045. [CrossRef]

9. Belviso, C.; Piancastelli, A.; Sturini, M.; Belviso, S. Synthesis of composite zeolite-layered double hydroxides using ultrasonic neutralized red mud. *Micropor. Mesopor. Mat.* **2020**, *299*, 110108. [CrossRef]

10. Li, X.Y.; Jian, Y.; Liu, X.Q.; Shi, L.Y.; Zhang, D.Y.; Su, L.B. Direct synthesis of zeolites from a natural clay, attapulgite. *Acs. Sustainable. Chem. Eng.* **2017**, *5*, 6124–6130. [CrossRef]

11. Anuwattana, R.; Balkus, K.J.; Asavapisit, S.; Khummongkol, P. Conventional and microwave hydrothermal synthesis of zeolite ZSM-5 from the cupola slag. *Micropor. Mesopor. Mat.* **2008**, *111*, 260–266. [CrossRef]

12. Li, C.X.; Zhong, H.; Wang, S.; Xue, J.R.; Zhang, Z.Y. A novel conversion process for waste residue: Synthesis of zeolite from electrolytic manganese residue and its application to the removal of heavy metals. *Colloid. Surface. A* **2015**, *470*, 258–267. [CrossRef]

13. Novembre, D.; Sabatino, B.D.; Gimeno, D.; Garcia-Vallès, M.; Martínez-Manent, S. Synthesis of Na–X zeolites from tripolaceous deposits (Crotone, Italy) and volcanic zeolitised rocks (Vico volcano, Italy). *Micropor. Mesopor. Mat.* **2004**, *75*, 1–11. [CrossRef]

14. Lee, C.H.; Lee, M.G. Removal of Cu and Sr ions using adsorbent obtained by immobilizing zeolite synthesized from Jeju volcanic rocks in Polyacrylonitrile. *J. Environ. Sci. Int.* **2018**, *27*, 1215–1226. [CrossRef]

15. Ayele, L.; Pérez-Pariente, J.; Chebude, Y.; Diaz, I. Synthesis of zeolite A using kaolin from Ethiopia and its application in detergents. *New. J. Chem.* **2016**, *40*, 3440–3446. [CrossRef]

16. Mohamed, R.M.; Ismail, A.A.; Kini, G.; Ibrahim, I.A.; Koopman, B. Synthesis of highly ordered cubic zeolite A and its ion-exchange behavior. *Colloid. Surf. A* **2009**, *348*, 87–92. [CrossRef]

17. Liu, H.B.; Peng, S.C.; Shu, L.; Chen, T.H.; Bao, T.; Frost, R.L. Magnetic zeolite NaA: Synthesis, characterization based on metakaolin and its application for the removal of Cu^{2+}, Pb^{2+}. *Chemosphere* **2013**, *91*, 1539–1546. [CrossRef]

18.   Li, C.X.; Zhong, H.; Wang, S.; Xue, J.R.; Zhang, Z.Y. Removal of basic dye (methylene blue) from aqueous solution using zeolite synthesized from electrolytic manganese residue. *J. Ind. Eng. Chem.* **2015**, *23*, 344–352. [CrossRef]

19.   Kim, S.R.; Lee, J.H.; Kim, Y.T.; Riu, D.H.; Jung, S.J.; Lee, Y.J.; Chung, S.C.; Kim, Y.H. Synthesis of Si, Mg substituted hydroxyapatites and their sintering behaviors. *Biomaterials* **2003**, *24*, 1389–1398. [CrossRef]

20.   Kuwahara, Y.; Ohmichi, T.; Mori, K.; Katayama, I.; Yamashita, H. Synthesis of zeolite from steel slag and its application as a support of nano-sized TiO2 photocatalyst. *J. Mater. Sci.* **2008**, *43*, 2407–2410. [CrossRef]

21.   Sugano, Y.; Sahara, R.; Murakami, T.; Narushima, T.; Iguchi, Y.; Ouchi, C. Hydrothermal synthesis of zeolite A using blast furnace slag. *ISIJ Int.* **2006**, *45*, 937–945. [CrossRef]

22.   Zhang, M.; Zhang, H.; Dan, X.; Lu, H.; Tian, B. Ammonium removal from aqueous solution by zeolites synthesized from low-calcium and high-calcium fly ashes. *Desalination* **2011**, *277*, 46–53. [CrossRef]

23.   Wang, W.Q.; Feng, Q.M.; Liu, K.; Zhang, G.F.; Liu, J. A novel magnetic 4A zeolite adsorbent synthesised from kaolinite type pyrite cinder (KTPC). *Solid. State Sci.* **2015**, *39*, 52–58. [CrossRef]

24.   Li, C.X.; Li, X.; Yu, Y.; Zhang, Q.W.; Li, L.; Zhong, H.; Wang, S. A novel conversion for blast furnace slag (BFS) to the synthesis of hydroxyapatite-zeolite material and its evaluation of adsorption properties. *J. Ind. Eng. Chem.* **2021**, *105*, 63–73. [CrossRef]

25.   Wan, X.K. Synthesis and characterization of composite molecular sieves with mesoporous and microporous structure from ZSM-5 zeolites by heat treatment. *Micropor. Mesopor. Mat.* **2003**, *62*, 157–163.